Development and characterization of Aluminium AA7075 hybrid composite foams (AHCFs) using SiC and TiB2 Reinforcement

Nitish Kumar Singh (hknitish@gmail.com)
VIT Bhopal University https://orcid.org/0000-0002-1160-4446
Balaguru Sethuraman

Research Article

Keywords: Aluminium hybrid composite foam, AA7075/SiC/TiB2, microstructural properties, oyster-shell powders, reinforcement, stirring temperature, top-loaded bottom pouring stir casting technique

Posted Date: July 26th, 2022

DOI: https://doi.org/10.21203/rs.3.rs-1718478/v1

Development and characterization of Aluminium AA7075 hybrid composite foams (AHCFs) using SiC and TiB_2 reinforcement

Nitish Kumar Singh[1], Balaguru Sethuraman[2*]

[1,2] School of Mechanical Engineering, VIT Bhopal University, Sehore, Madhya Pradesh, 466114, India

* balaguruiitm@gmail.com, iitmguru239@gmail.com
+919444465649

ABSTRACT

In this study AA7075/SiC/TiB_2 closed-cell Aluminium hybrid composite foam (AHCFs) with different densities was fabricated by top-loaded bottom pouring stir casting technique. This technique uses oyster-shell powders ($CaCO_3$ 2.5 wt. % of composite with 60 μm size) as blowing agents and no viscosity-enhancing ingredient. The silicon carbide (SiC 0, 3, 6, 9, and 12 wt. % with 25 μm) and titanium di-boride (TiB_2 3 wt. % with particle size 15 μm) are used as primary and secondary reinforcement agents. It has been noted that the addition of TiB_2 and SiC enhanced the mechanical properties (modulus of elasticity, yield strength, and plateau strength) of AHCFs. The energy absorption capacity of AHCFs increases with the addition of SiC up to 3 wt. % and a further increase in SiC content leads to the reduction. It is observed that density and cell wall thickness increases with increasing the wt. % of SiC and Cell size and porosity decrease with an increase in wt. %. of reinforcement. It is also noted that Stirring temperature also strongly influenced the microstructural properties of AHCFs, and 750 ^{0}C of stirring temperature is sufficient for aluminium foaming.

Keywords: *Aluminium hybrid composite foam, AA7075/SiC/TiB_2, microstructural properties, oyster-shell powders, reinforcement, stirring temperature, top-loaded bottom pouring stir casting technique*

1. INTRODUCTION

Aluminium and their alloys foams have received much attention in recent years because of their extremely low density and unique functional properties, such as their ability to influence energy absorption, sound absorption, and flame resistance [1]. Aluminium Metal foams exhibit mechanical and physical characteristics, such as lightweight, high explicit stiffness, excellent strength-to-weight ratios, and massively increased energy absorption capabilities, which make them beneficial in the automotive and aviation industries [2]. Foams of aluminium metal can be produced in a variety of ways, such as through stir casting methods [3][4][5], powder metallurgy process [6], sintering method [7], foaming compact blowing agents, the building of gas in melt injection employing foaming agents. Direct and indirect foaming processes may fabricate it. Direct foam techniques start with molten metal containing equally scattered non-metallic particles, which produce a gas injected to create foam [8]. Methods of indirect foaming begin with a solid precursor

from which a dispersed blowing agent is uniformly dispersed in an aluminum matrix [9]. According to their cell morphology, metal foam can be classified into two categories: closed-cell foam and open-cell foam. Open-cell foams are interconnected only by their edges in contrast to closed-cell metal foams, which are separated by their cell walls [10]. The applications of open-cell foams are possible in bone implants, heat exchangers, filters, etc. The close cell foams are used for energy absorption, sandwich panels, and thermal insulation [11][12]. The demand for closed-cell aluminium foam has increased in the defence and automobile industries due to its good physical and mechanical properties[13]. Stir casting is generally preferred over other manufacturing methods of metal matrix composites foams [14]. It is an economical route of composite and foam preparation and offers ease of production. Due to this, it was used by various researchers for the processing of Aluminium matrix composites and aluminium matrix composite foams [15][16][17]. Therefore, the stir casting route was used in the current research for the fabrication of hybrid composites and hybrid composite foam. In this method, the wettability of reinforcements with the matrix alloy is a major problem. This difficulty was handled by incorporating oyster-shell powder ($CaCO_3$) as a foaming agent and SiC, TiB_2 as a reinforcing agent, which improves the wettability of aluminium reinforcement. Researchers have conducted many studies to improve the mechanical attributes of existing foams, producing novel classes of high-strength hybrid composite foams to enhance their applications. Different types of reinforcement like metallic, ceramic [18], and carbonaceous[19]were widely used for enhancing the performance of aluminium composites foam. For the development of hybrid composite foams, alloy composition has a significant impact on both foamability and mechanical properties of metal foams, both of which have an impressive effect on energy absorption and compressive strength. So a composite's foam properties are significantly influenced by its material selection. AA7075 exhibits good mechanical strength, corrosion resistance, fatigue strength and creep resistance compared to pure aluminium among all the aluminium series. It offers the highest strength and potential for dry sliding wear applications [20][21][22]. Researchers reported the mechanical properties of various aluminium series, which indicates that AA7075 has the highest strength, hardness, and the lowest wear rate of all aluminium series, i.e., 1xxx, 2xxx, 3xxx, 6xxx, and 7xxx[23]. Due to its low weight-to-strength ratio, high wear resistance, and creep resistance, it has potential applications in the automotive, aeronautical, sports, and electronics[24]; therefore, aluminium 7075 alloy was selected as the matrix material for the preparation of hybrid composite foam. In hybrid composites foams, mainly two types of reinforcement are used, namely primary and secondary reinforcement. Synthetic ceramics are used as primary reinforcements as they possess superior strength compared to other types of reinforcements. However, secondary reinforcement is frequently used to improve other properties, such as thermal conductivity, friction coefficient, and strength-to-weight ratio [25][26][27]. In this study, silicon carbide (SiC) (chemically stable with aluminium) is used as primary reinforcement and titanium-di-boride (TiB_2) as secondary reinforcement. The TiB_2 establishes an appropriate bond with the matrix without forming intermetallic phases.

Many researchers work on closed-cell aluminium foam. However, there is still an insufficient volume of research on Al composite foaming mechanisms, limiting the knowledge related to the

factors and parameters that determine the formation of foams with consistent quality. Also, the control of structure and morphology remains a challenging task. Previous research has not provided a better understanding of the influence of various reinforcement weight percentages on the microstructural and mechanical characteristics of aluminium hybrid composite foam (AHCFs). Reinforcement and their compositions have a significant role in both composite and foam's mechanical properties, which have an impressive effect on microstructure, compressive deformation, and energy absorption. Therefore, in this research, closed-cell, aluminium hybrid composite foam AA7075+ x % by weight of SiC (x= 0, 3, 6, 9, and 12) + 3 % by weight of TiB_2 was prepared by stir casting technique using oyster-shell powder as a foaming agent without any viscosity-enhancing agent. The effect of the reinforcement agent on the microstructural properties (cell size, cell wall thickness, cell circularity) and compressive deformation mechanism (yield strength, pleatue stress, and energy absorption capacity) was analyzed.

2. EXPERIMENTAL DETAILS

2.1. Material and Methods

The closed-cell aluminium/SiC/TiB_2 foams with relative densities(ρ_{rd}) from 0.184 - 0.434 were fabricated by melt foam method (stir casting technique shown in Figure 1A) using oyster-shell powder ($CaCO_3$) as foaming agent and without any thickening agent. The AA7075 matrix contains 6.60 wt. % Zn, 2.54 wt. % Mg, 1.63 wt. % Cu, 0.22 wt. % Cr, 0.06 wt. % Si, 0.18 wt. % Fe and 89.77 wt. % Al.

1. 1.5 kg Ingot of fabricated AA7075+ XSiC (X= 0, 3, 6, 9 and 12 % wt.) + 3 wt. % TiB_2 composite was cleaned by acetone which are called charge.
2. Five cleaned pieces were kept inside a cylindrical crucible.
3. Five charges with different percentages of reinforcements are shown in table 1; the aluminum alloys were melted in the stir casting electric furnace at a temperature of 810°C.
4. We added 30 grams of flux to the molten alloy, stirred it for 5 minutes at 550 RPM to remove impurities, and lowered the temperature to 770^0C.
5. Heat-treated oyster-shell powder (2.5 wt. %, with a particle size of 60 μm)) is added to different charges and stirred for 10 minutes at different string temperatures to obtain uniform powder distribution.
6. The melt remains in the furnace after stirring, allowing the $CaCO_3$ to decompose into carbon dioxide (CO_2), responsible for foam generation.
7. Figure 1(b) shows that the crucible was taken out of the furnace and cooled by the atmospheric air to solidify the foam.
8. The foam samples are prepared by machining process after solidification for characterization and testing.

Table 1. Composition of Fabricated Aluminium matrix (AA7075) Hybrid composite foam

Sample	Matrix	Reinforcement	
		SiC wt%	TiB_2 wt. %
ACFs	AA7075	0	0
AHCFs-A	AA7075	3	3
AHCFs-B	AA7075	6	3
AHCFs-C	AA7075	9	3
AHCFs-D	AA7075	12	3

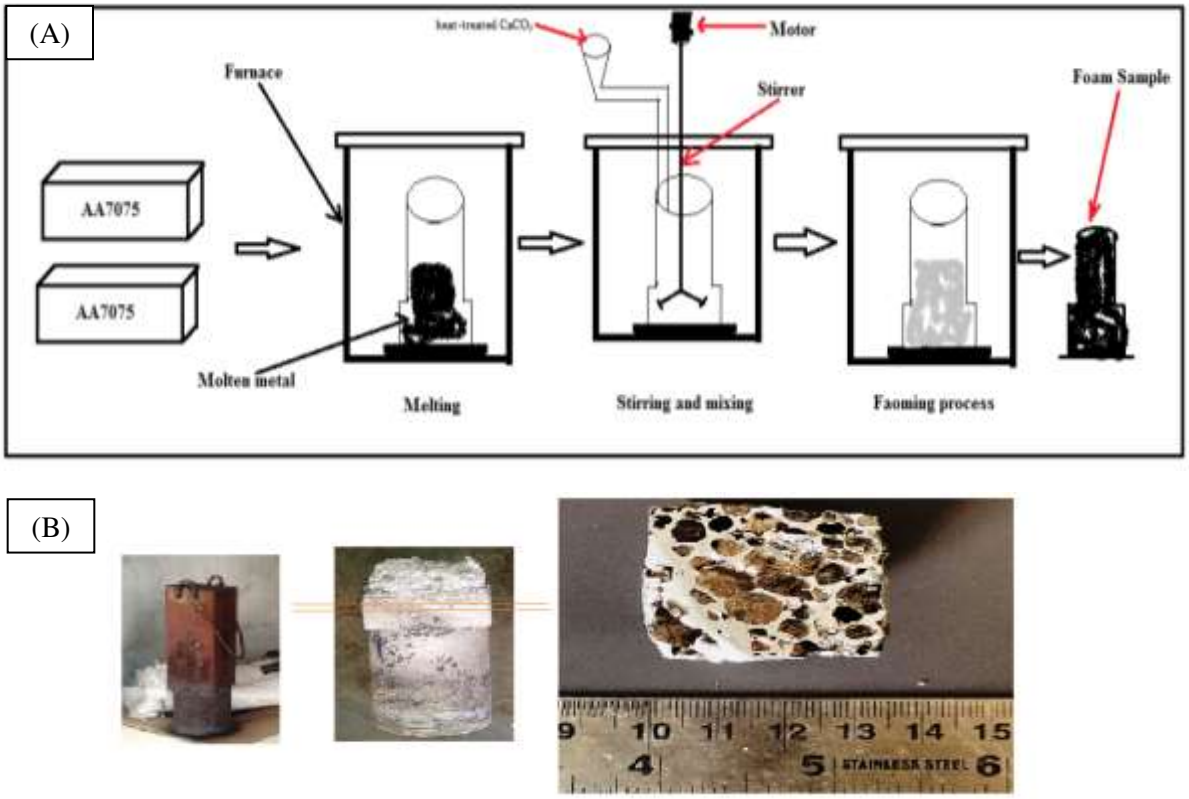

Figure 1. Procedure for Fabrication of Aluminium Foam (A) by stir casting method (B) Mould and produced foam

2.2. Relative Density and Microstructure

After fabricating the foams, the samples were cut by EDM wire Machine into an approximate size of 30mm×30mm×30mm for all tests. Figure 2 Represents the Cross-section of Aluminium Hybrid Foam samples (AHCFs). All samples' density, relative density (ρ_{rd}), and porosity were calculated using the equations 1, 2, and 3.

$$\rho = \frac{m}{v} \qquad (1)$$

$$\rho_{rd} = \frac{\rho_{foam}}{\rho_{solid}} \quad (2)$$

$$\% \text{ of porosity } = 1 - \rho_{rd} \times 100 \quad (3)$$

Where ρ is the density of the samples in g/cc, m is the weight of the samples (gm.), v is the volume of the samples, and ρ_{rd} is the relative density of foam samples. As foams contain voids, the conventional method cannot calculate their volume. The volume of porous material can be measured using Archimedes' principle. A detailed procedure for evaluating the volume of porous material has been described in the literature [28].

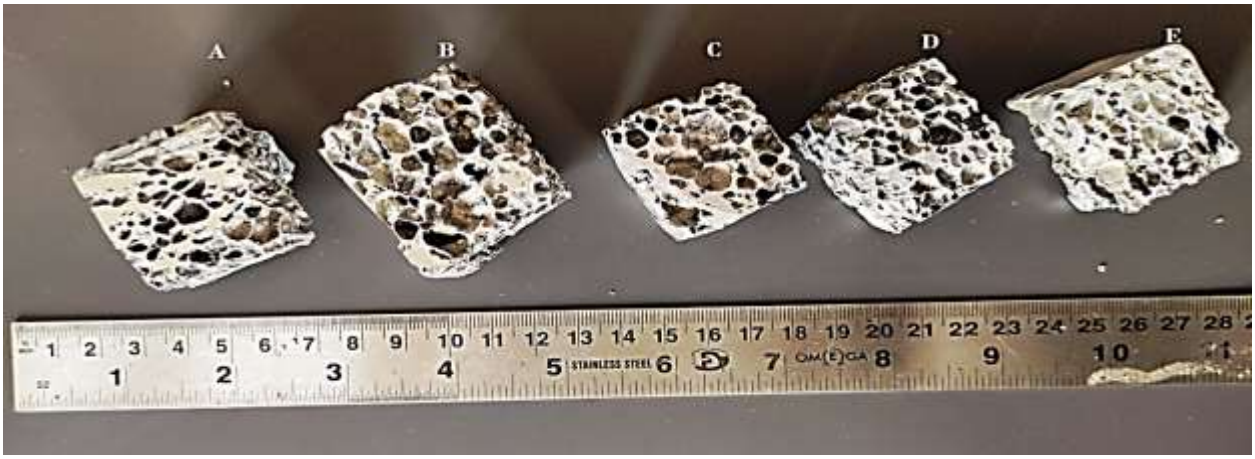

Figure 2. Cross-section of Hybrid Aluminium Foam samples (A) 0% wt of SiC and TiB_2 (B) 3 % wt of SiC and TiB_2 (C) 6 % wt. of SiC and 3 wt. % of TiB_2 (D) 9 % wt. of SiC and 3 wt. % of TiB_2 (E) 12 % wt. of SiC and 3 wt. % of TiB_2

To examine the microstructure of the samples, standard metallographic techniques were used to polish and etch the samples. Energy dispersive x-ray spectroscopy (EDS) is an analytical technique used to analyze a sample's chemical composition and elemental composition. A unique atomic structure is associated with every element, and the main principle of spectroscopy is based on that unique structure. In the present work, EDS was carried out in the microstructure analysis of the sample through scanning electron microscopy (SEM model no. ZEISS EVO 18). The EDS analysis of a sample is carried out at different portions such as the plateau region, cells region, and cell walls region of hybrid composite foam samples. Microstructural properties such as cell size, cell wall thickness, and circularity of AHCFs were determined using ImageJ software [29].

2.3. Deformation Mechanism

For the deformation mechanism of AHCFs, Compression test samples were cut (25mm×25mm×25mm) in cubical shape, and faces were flatted on the belt grinding machine so that samples could not wobble during compression testing. A quasi-static compression test was

conducted at room temperature using a universal testing machine (UTM) (TUE/C-400) at a strain rate of 0.01/s. Stress-strain graphs were generated using a standard methodology based on load-displacement data recorded during the test. We determined plateau stress, densification strain, and energy absorption using compressive stress-strain curves.

2.4. Energy absorption

The amount of energy absorbed by metal foams under compressive loading is described as the area under the stress-strain curve up to ε_D. The Energy absorption(E_{ab}) of Aluminium foam is calculated from stress-strain response curve, it can be mathematically expressed by the following relation [30].

$$E_{ab} = \int_0^{\varepsilon_D} \sigma_{pl} d\varepsilon \qquad (4)$$

Whereσ_{pl} and ε_D are the plateau stress and densification strain. Therefore, the E_{ab} (in Eq. 1) of Aluminium, foam is the function of ε_D and σ_{pl}, also these properties depend on the relative density (ρ_{rd}) of aluminium foam.

The energy absorption efficiency (ξ_{ab}) of aluminium foam calculated by the following relation;

$$\xi_{ab} = \frac{E_{ab}}{(\sigma_{max} \cdot \varepsilon_D)} \times 100 \qquad (5)$$

Where σ_{max}, σ_{pl} and ε_D are analogous to the peak stress, plateau stress and densification strain.

2.5. Micro-hardness Testing

To determine the hardness of the prepared foam samples, a Rockwell hardness test was conducted on the AHCFs cell wall using a Rockwell hardness machine (FIE make Model IRB-250) by loading 100Kgf on the Rockwell hardness machine(FIE make Model IRB-250). For this experiment, a 1/16 diamond ball indenter is indented into the cell wall to determine the hardness of the AHCFs.

3. RESULT AND DISCUSSION

3.1. Relative Density and Porosity

By applying equation 1, we can determine the density of the ACFs and AHCFs and measured to be 1.15 g/cc and the range 0.51-1.2 g/cc depending upon the reinforcement content, respectively. The relative density and percentage of porosity are calculated using equations 2 and 3, shown in table 2. It is observed from Table 2 that Pure AA7075 (unreinforced ACFs) with 59.074 % porosity and AHCFs-1, AHCFs-2, AHCFs-3, AHCFs-4 with 81.52, 76.81, 75.36, and 56,52 % porosity respectively is significantly high as compared to pure AA7075 ACFs except AHCFs-4 (12wt % of SiC) which is mainly due to hybrid composite foams AA7075 (up to 9 wt. % of SiC) exhibit more uniform pore structure than pure AA7075 foams and exhibit non uniform pore distribution beyond the 9 wt. % of SiC. When the weight of primary reinforcement SiC increases from 3-12

wt. %, the porosity is reduced from 81.52 to 56.52; because of the high viscosity of molten metal, fewer voids form in metal foam.

3.2. Microstructure

The SEM image of foams with the different percentage by weight of silicon carbide and 3 % by weight of titanium di-boride (TiB_2) is shown in Figure 3. It can be observed that each cell is divided with a closed boundary called a cell wall. SEM images were examined, and the cell structure was analyzed via ImageJ software by following steps; firstly, an SEM image was imported into the software. The pixels in the image are translated into the distance, and subsequent calculations are made using that distance. To examine cell size and wall thickness and obtain information about the individual cells in all types of AHCF samples, 50 unique cells were selected. Figure 4 illustrates the frequency distribution of AHCF sizes, and Table 2 provides cell information for all the samples at the stirring temperature (750^0C). It is also observed that the porosity within the cell walls is present due to the presence of reinforcement particles, and these porosities are uniformly distributed. Due to the presence of reinforcement particles, we also observed the presence of porosity within the cell walls, which is uniformly distributed, and an alumina-silicate phase structure was developed. It was deduced that the eutectic silicon needles pushed the TiB_2 particles toward the cell boundaries. Additionally, there is a strong interfacial bond between reinforcements and matrix materials. This strong interfacial bonding may be caused by the alumina-silicate phase present in matrix materials which will help load transfer from the matrix to reinforcement.

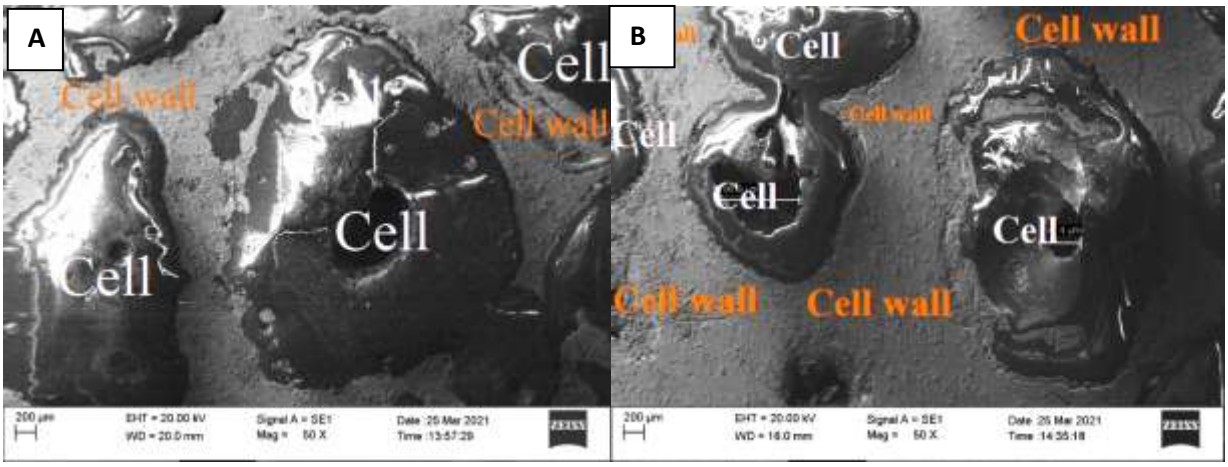

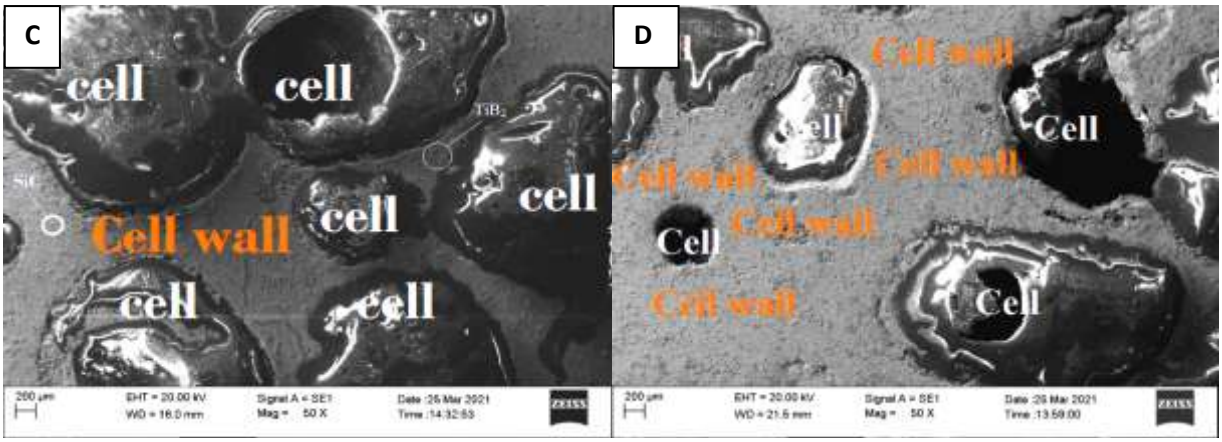

Figure 3. Scanning electron microscope images (A) 3 % wt of SiC and TiB_2 (B) 6 % wt of SiC and 3 wt. % of TiB_2 (C) 9 % wt. of SiC and 3 wt. % of TiB_2 (D) 12 % wt. of SiC and 3 wt. % of TiB_2

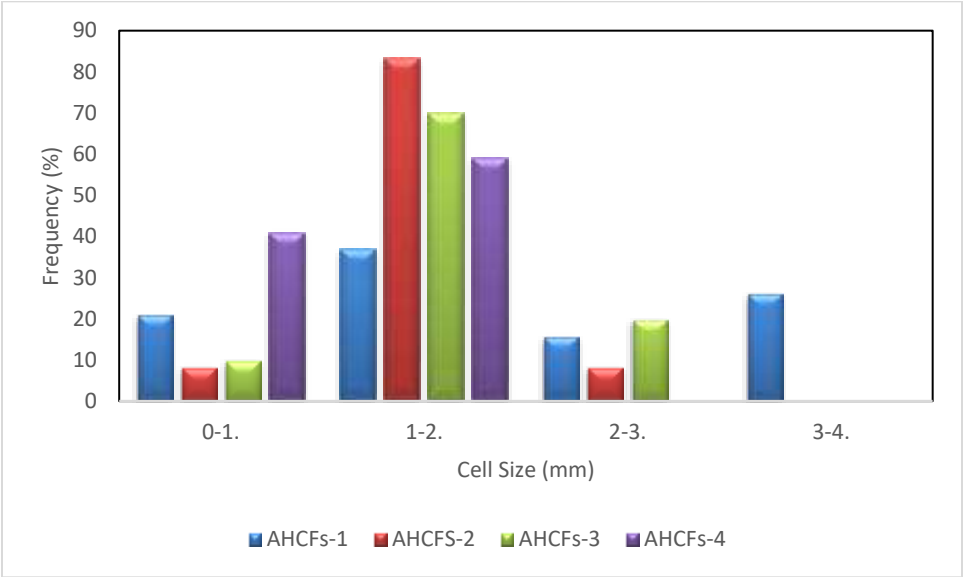

Figure 4. Cell size distribution of AHCFs at 750^0C foaming temperature

Table 2. Physical properties and cell information of the AHCFs

Sample	Density (g/cc)	Relative density	% Porosity	cell size (mm)	cell wall thickness (µm)
AF	1.15	0.409253	59.074	1.12	802.32
AHCFs-1	0.51	0.184783	81.521	1.98	459.69
AHCFs-2	0.64	0.231884	76.811	1.588	549.6
AHCFs-3	0.68	0.246377	75.362	1.51	569.7
AHCFs-4	1.2	0.434783	56.521	1.033	877.88

3.2.1. Effect of wt. % of reinforcement on physical and microstructure properties

It can be observed from table 2 that the relative density of reinforced AHCFs is minimum, as well, as the cell size of AHCFs is maximum for the alloy with 3 wt. % of SiC (AHCFs-2), which means that the maximum foamability occurs in the AHCFs-2, that's indicate increasing the wt. % of primary reinforcement SiC while keeping the wt. % of secondary reinforcement TiB_2 constant (3 wt. %), the cell size reduced, and cell wall thickness increased. From figure 5, it is clear that increasing the weight percentage of SiC from 3 to 9 wt. %, the pore size decreased from 1.98 mm to 1.51 mm, more than the unreinforced Aluminium composite foam (ACF). This means the foambility of the AHCFs also increased by adding SiC reinforcement compared to ACF (unreinforced), but the pore size of AHCFs-4 is lower than the pore size of ACF (unreinforced foam). In other words, the viscosity of the melt is too high, and surface tension is low at 12 wt. %, which clearly shows that silicon carbide acts as a viscosity-enhancing agent. In AHCFs-4, the cell wall thickness between pores is thick. Due to improper foaming, a lower number of significant pores or cells were observed. SiC 9 % reinforcement particles exhibit significant increment and hence, sufficient for obtaining the foam. The above result shows that SiC (9 % by wt.) help to increase of expansion rate. Further, an increase in the wt. % of SiC reduces the cell size and increases cell wall thickness. This indicates that the expansion is very low. So, SiC 3-9 wt. % is useful for AA7075/SiC/TiB_2 AHCFs.

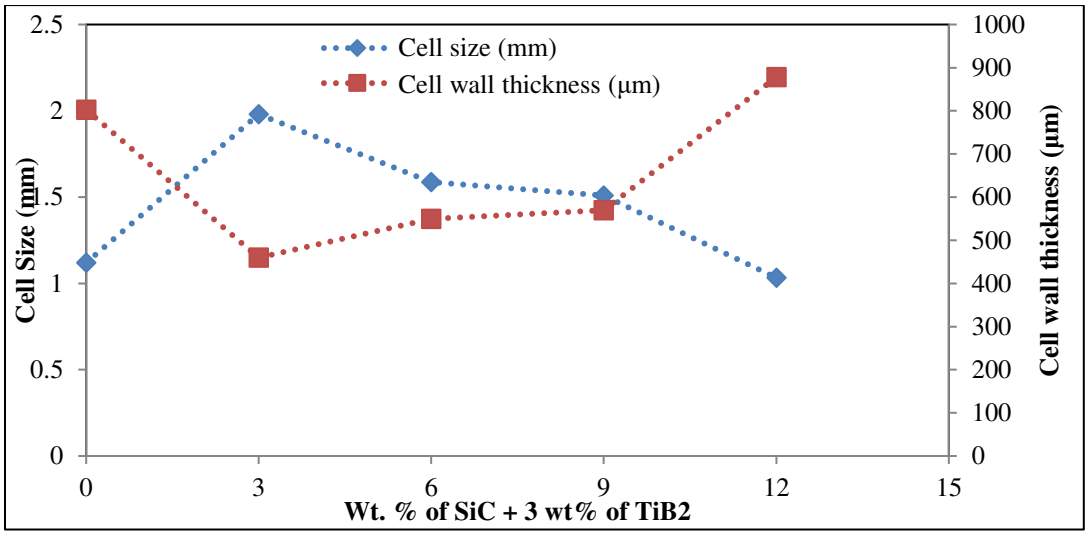

Figure 5. Effect of wt. percentage of the reinforced particle on cell size and cell wall thickness.

3.2.2. EDS Analysis

Figure 6 (A-C) shows the microstructure and EDS spectrum of AHCFs-2 foam specimen at different locations within the foam cell and cell wall. Figure 6 (A) shows that the matrix is made of Al-Si-Ti alloy, containing traces of metals such as magnesium, copper, and zinc. As a result of the TiB_2 reinforcement utilized in the matrix material, titanium (Ti) is present in the EDS. Figure 6 (B) showed SiC and TiB_2 presence within the cell wall. The EDS taken on the cell wall shows the presence of Mg, Cu, and Zn as major constituents and Fe as minor. The

EDS spectra on the cell and cell wall interface indicate that the reinforcement particles were uniformly distributed in the AA7075 aluminium composite with strong intermolecular bonding. Figure 7 shows the elemental mapping of the AHCFs-2 sample at the cell and cell wall interface. The cell wall and cell interface of AHCFs typically contained C, O, Mg, Al, Si, Fe, Cu, Zn, Ca, and Ti.

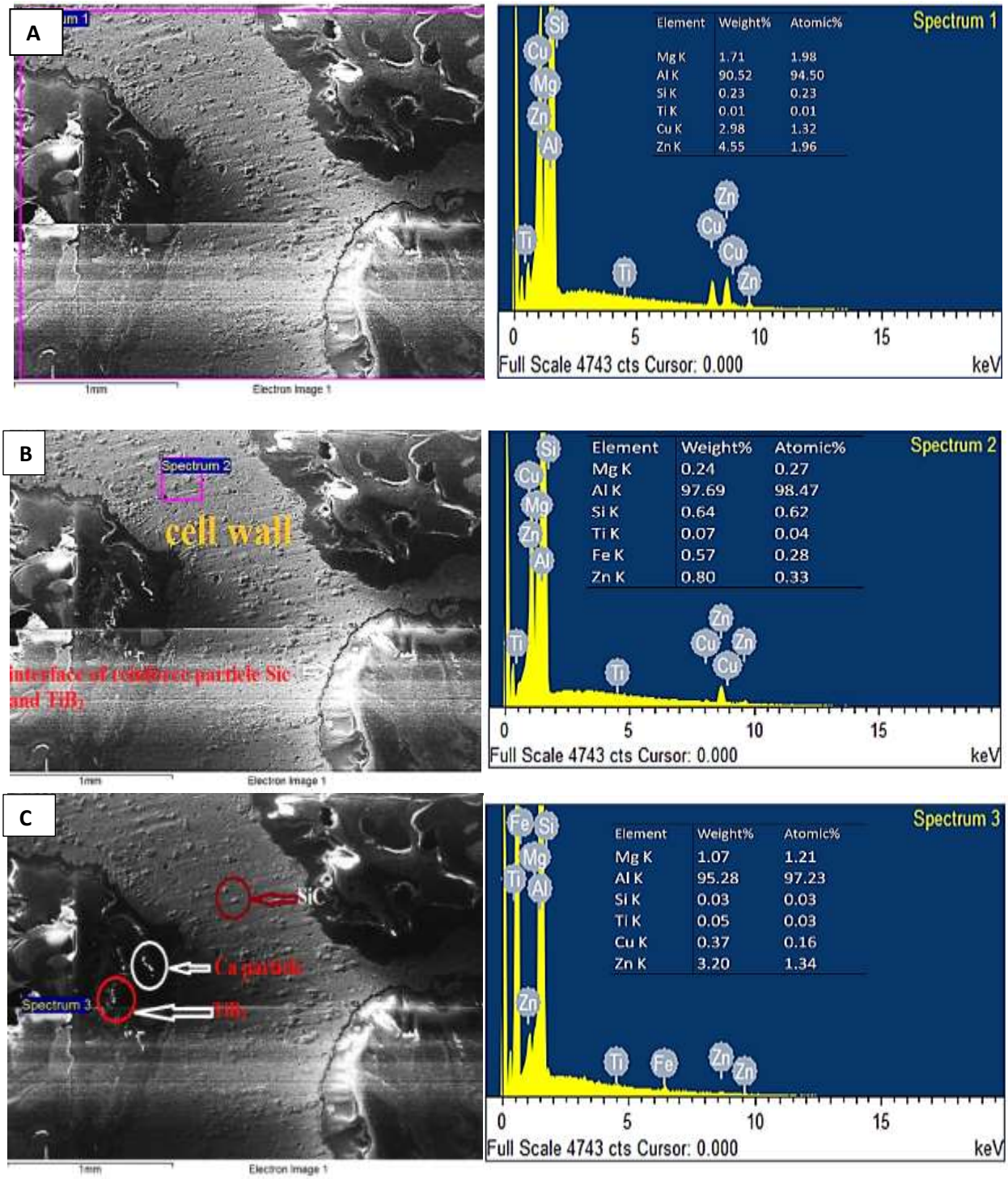

Figure 6. Microstructure and EDS image of AHCFs-2 sample: (a) spectrum of near to the cell wall (b) spectrum of cell wall matrix material and (c) at the interface of Cell matrix material.

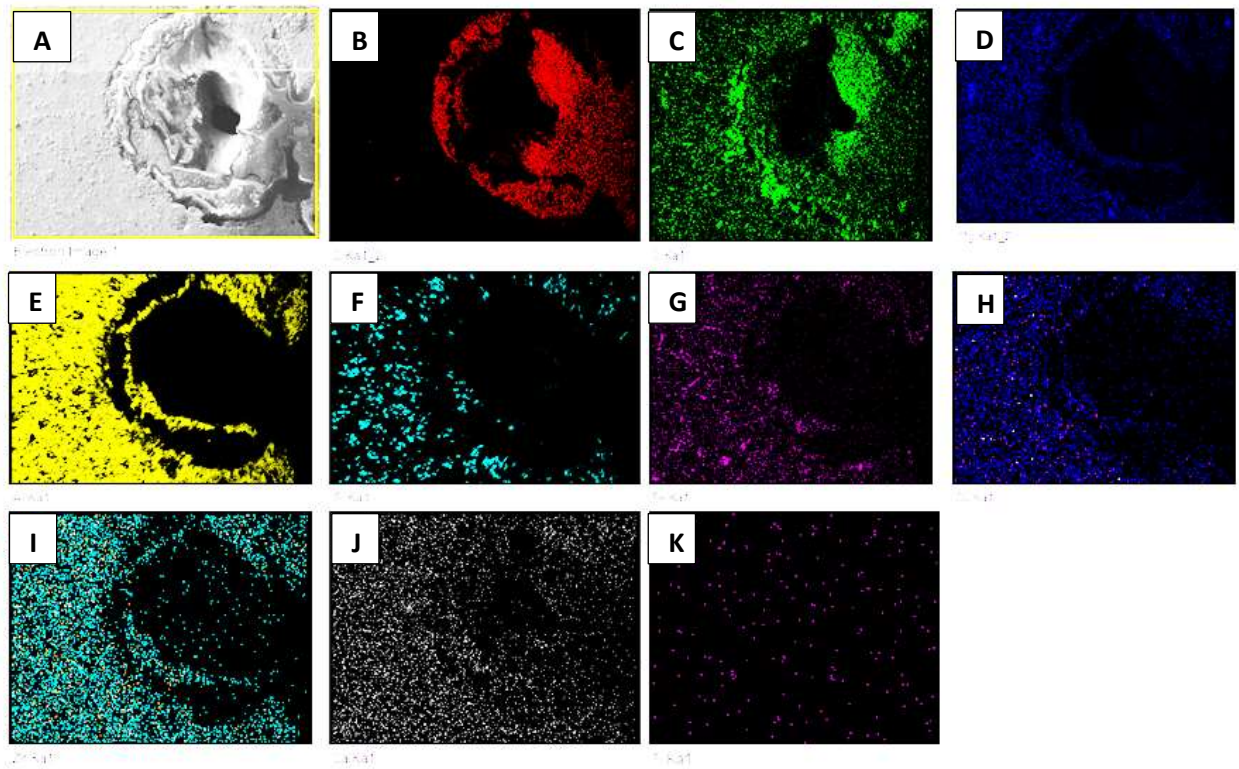

Figure 7. Elemental mapping of AHCFs-2 foams sample (A) SEM image (B) distribution of carbon (C) distribution of oxygen (D) distribution of magnesium (E) distribution of aluminium (F) distribution of silicon (G) distribution of iron (H) distribution of copper (I) distribution of zinc (J) distribution of calcium (K) distribution of titanium

3.2.3. Effect of stirring temperature on physical and microstructure properties

Figures 8 and 9 show the effect of stirring temperature and the wt. % of primary reinforcement SiC (0, 3, 6, 9 and 12) keeping constant wt. % of secondary reinforcement on the density and porosity of the AHCFs. The density of AHCFs under experimental conditions varies from 0.49 to 1.57 (porosity 82.44 to 43.11) depending upon the amount of SiC and the stirring temperature.

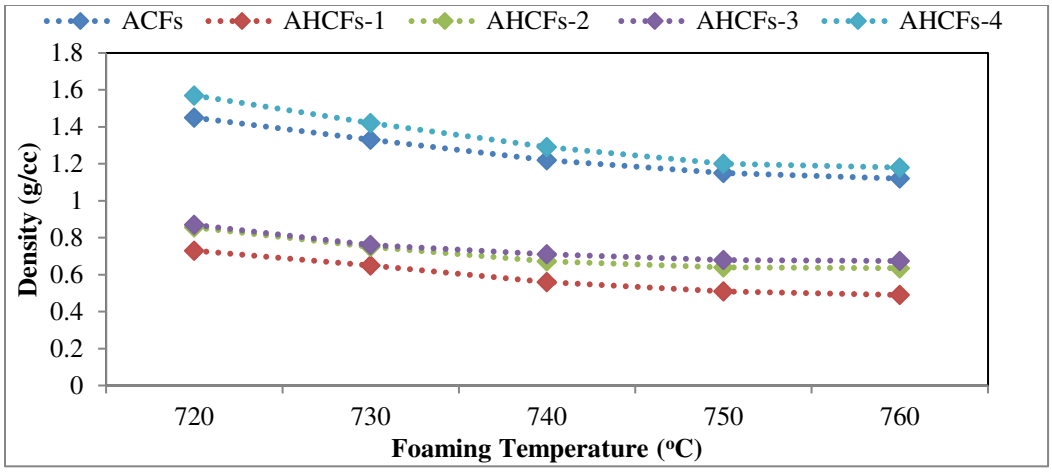

Figure 8. Effect of stirring temperature on density

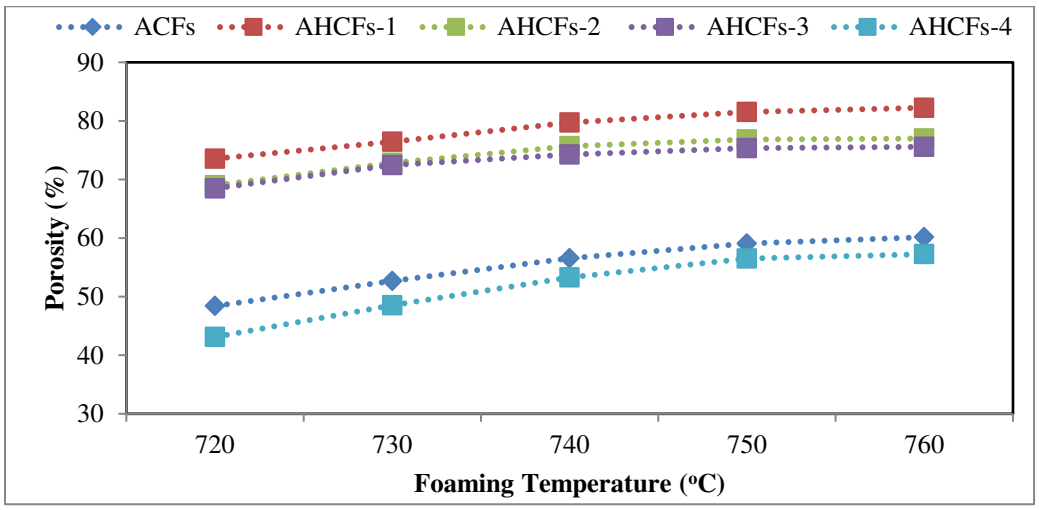

Figure 9. Effect of stirring temperature on porosity

Increasing the stirring temperature results in decreasing the density and increasing the porosity. By increasing the stirring temperature, the solubility of reinforcement is also increased. Therefore, the foam expansion increases when the stirring temperature increases, increasing the porosity. Figure 8 is divided into two sections: before and after 750^0C stirring temperature, the foam expansion rate of 720-750^0C increases significantly. However, after 750^0C, the expansion rate is almost constant. At stirring temperature from 720-750^0C, the decomposition rate is more of reinforcement SiC, TiB_2, and $CaCO_3$ foaming agent, and the melt is thicker. When the decomposition of the foaming agent is more, it releases more the carbon-di-oxide (CO_2) gas, which is responsible for poring generation; hence formability of the foam is increased. Considering the graph of AHCFs-1, density decreases from 0.56 to 0.51 in the stirring temp range of 740-750^0C; on the other hand, density decreases only from 0.51 to 0.49 in the range 750^0C-760^0C. It was observed that 750^0C of stirring temperature was sufficient for foaming AA7075/SiC/TiB_2.

3.3. Compressive stress-strain behavior

Each AHCFs was subjected to a quasi-static compression test; a uniaxial compression test was conducted to obtain the compressive stress-strain curve. Figure. 10 shows three distinct zone of deformation in a stress-strain curve.

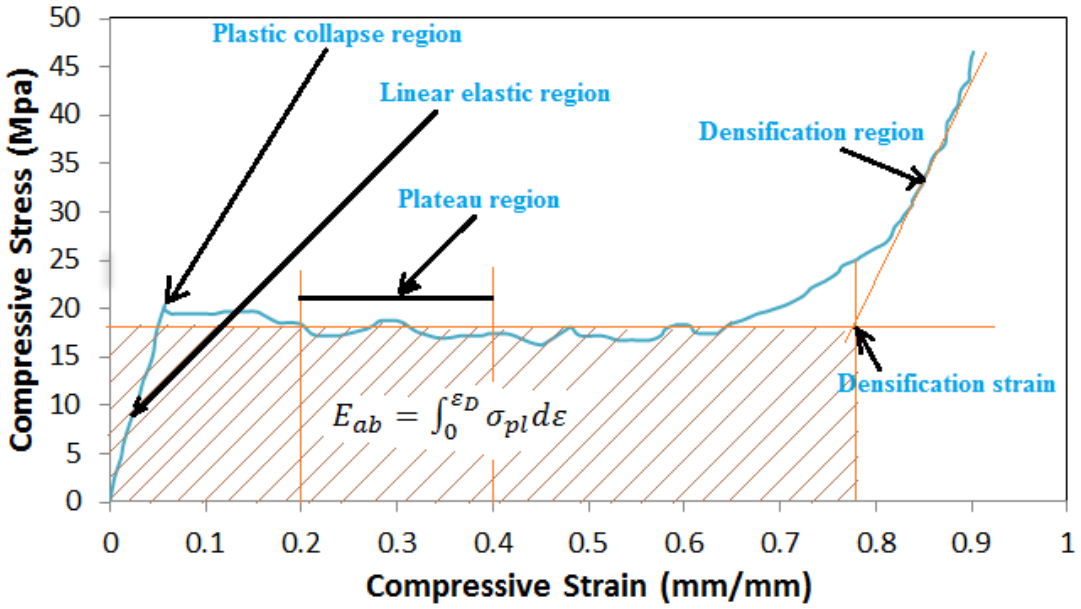

Figure 10. Nomenclature of Stress-strain curve

The compressive stress varies linearly with the strain up to yield strength classified under the first zone. The second zone is the Plateau region, in which compressive stress is almost constant with stain. It is calculated according to the ISO13314 standard, which states that the plateau stress is the average stress value between 0.2-0.4 strain levels. The third zone is the densification region; the stress suddenly increases with a small increment of strain that occurs due to the cell inside the foam structure being completely crushed. The Densification strain (ε_D) is the stain value at the corresponding junction point of the plateau line and the tangent drawn at maximum curvature on the densification region.

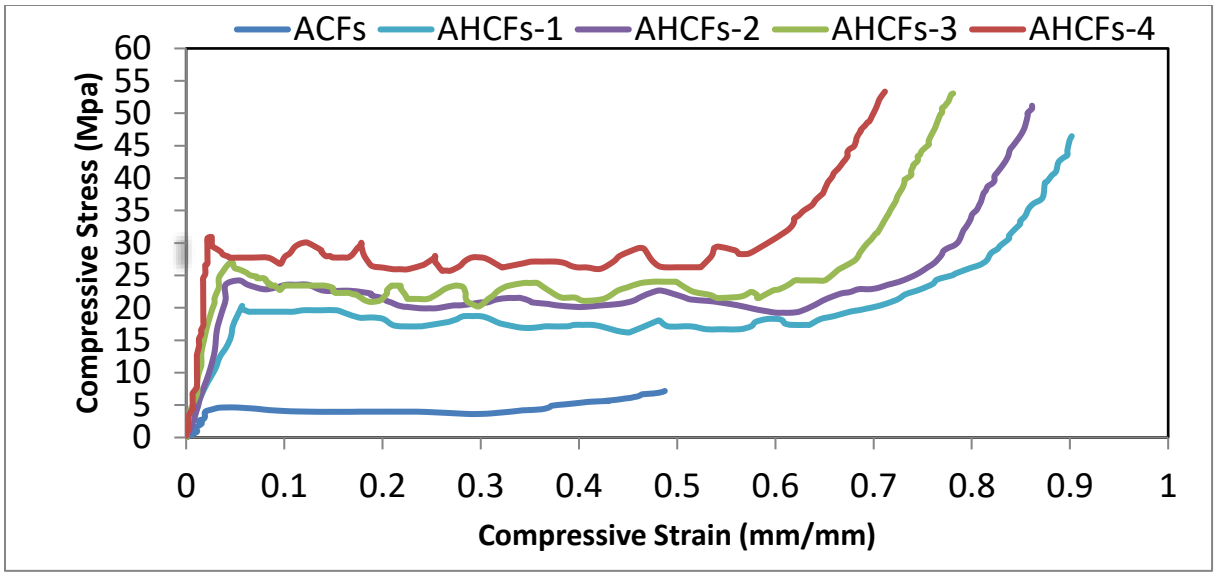

Figure 11. Compressive Stress-Strain curve

The compressive stress-strain curve of AA7075 foams with 0, 3, 6, 9, and 12 wt. % SiC and 3 wt. % of TiB_2 is shown in Figure 11. It is observed that all the curves share the same qualitative characteristics. The mechanical properties (σ_c,σ_{pl} ,$\varepsilon_D$and E_{ab}) of AHCFs for different samples are calculated from these stress-strain responses. Tests were conducted three times for each sample to get precise results, and the average values of the properties mentioned above from the tests were analyzed, as shown in Table 3

Table 3. Compressive properties of AHCFs

	E_c (GPA)	**σ_c (MPa)**	**σ_{pl} (MPa)**	**ε_D (mm/mm)**	**E_{ab} (MJ/m^3)**	**ξ_{ab} (in %)**	**Relative density**
ACFs	0.23	4.9	4.1	0.45	1.845	83.67	0.409253
AHCF-1	0.34	20.2	18.4	0.78	14.35	91.07	0.184783
AHCFs-2	0.66	24	21.7	0.765	16.60	90.41	0.231884
AHCFs-3	0.67	27.1	23.75	0.68	16.15	87.63	0.246377
AHCFs-4	1.55	31	25.2	0.61	15.37	81.27	0.434783

The elastic modulus(σ_c) of AHCFs is defined as the slope of the compressive stress-strain curve in the linear elastic region. AHCFs-4 (12 wt. % of SiC and 3 wt.% of TiB_2) has an elastic modulus, plastic collapse strength(σ_c) , and plateau strength(σ_{pl}) of about 6.74 %, 6.33 %, and 6.1 %, respectively, which are higher than that of unreinforced AA7075 (ACFs). Moreover, elastic modulus, plastic collapse strength, and plateau strength of AHCFs-4 are about 4.55 %, 1.53% and 1.36 % higher than that of AHCFs-1. Elastic modulus, plastic collapse strength, plateau strength of AHCFs-4 is 2.34 %, and 1.29 %, and 1.2 % higher than AHCHs-2. 2.31%. Elastic modulus, plastic collapse strength, and plateau strength of AHCFs-4 are 1.14 % and 1.06 % higher than AHCFs-3. The elastic modulus, plastic collapse stress, and Plateau stress of AHCFs-4 have the highest value due to its lower pore size, which means the lowest density, as the slope angle becomes larger when the pore size is reduced. These trends could be seen in all the samples. In

this experiment, the elastic modulus, yield stress, and Plateau stress depend on the reinforcement content, increasing with the primary reinforcement (SiC) content.

3.4. Energy Absorption

The samples' energy absorption was calculated using equation 4 and tabulated in Table 3. It is observed that AHCFs-2 (6 wt. % of SiC+3 wt. % of TiB_2) has the highest energy absorption, about 799.72%, which is higher than the pure AA7075 ACFs. AHCFs-2 and AHCFs-3 have nearly the same energy absorption, and AHCFs-4 exhibits lower energy absorption when compared to all reinforced AHCFs and higher than the pure AA7075 foam. The energy absorption has no particular trends in AHCFs-4 having higher Plateau strength; it is expected to have maximum energy absorption. Figure 12 shows that reinforcement content that influenced the energy absorption and its efficiency of AHCFs. The energy absorption of AHCFs increases with the increase in SiC content up to the 6 wt. % and a further increase in SiC lead to a reduction. Simultaneously, the energy absorption efficiency increases with the increase in SiC content up to 3 wt. % and a further increase in SiC, it decreases. The change in behavior is due to the differences in the non-homogeneity in the melt that's conforming to the homogeneity of the cell structure affected more the energy absorption.

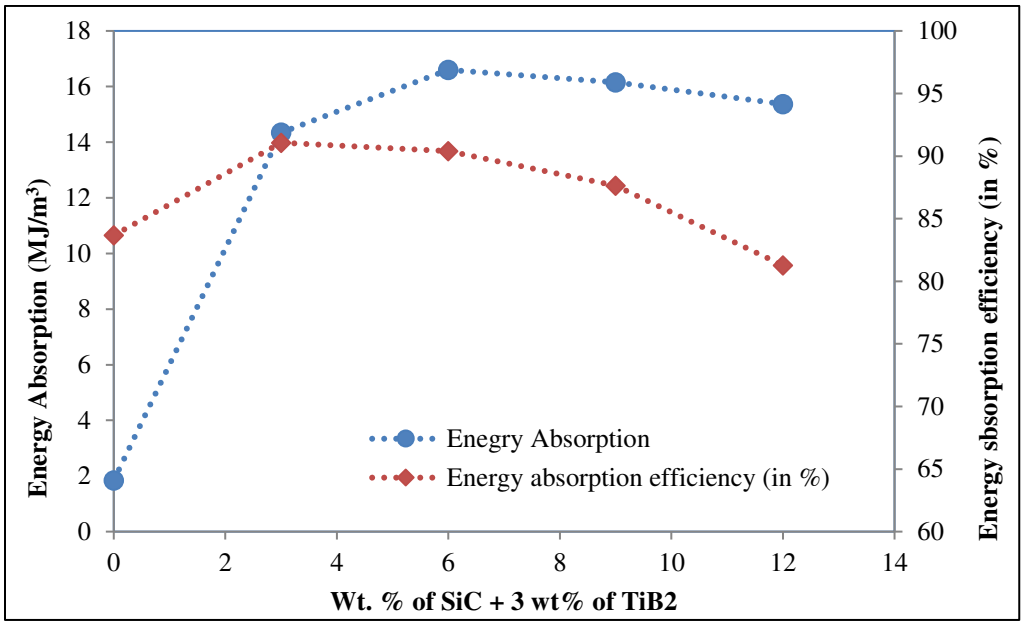

Figure 12. Variation of energy absorption and energy absorption efficiency with wt. % of reinforcement

3.5. Deformation mechanisms

The quasi-static compressive deformation mechanism of the cubical specimen was investigated with the help of their stress-strain response (Figure 13A) and corresponding digital pictures (Figure 13B), which are captured during deformation at different stages, as shown in Figure 13(a-g).

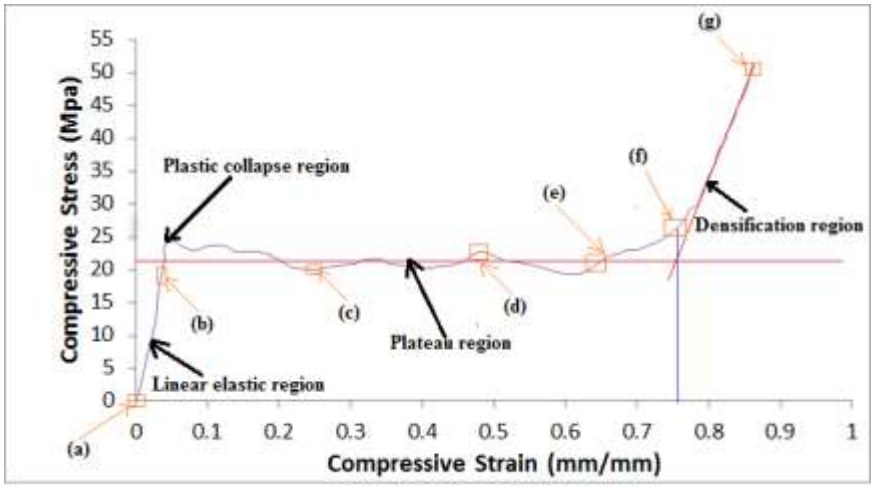

Figure 13 (A) Compressive stress-strain response

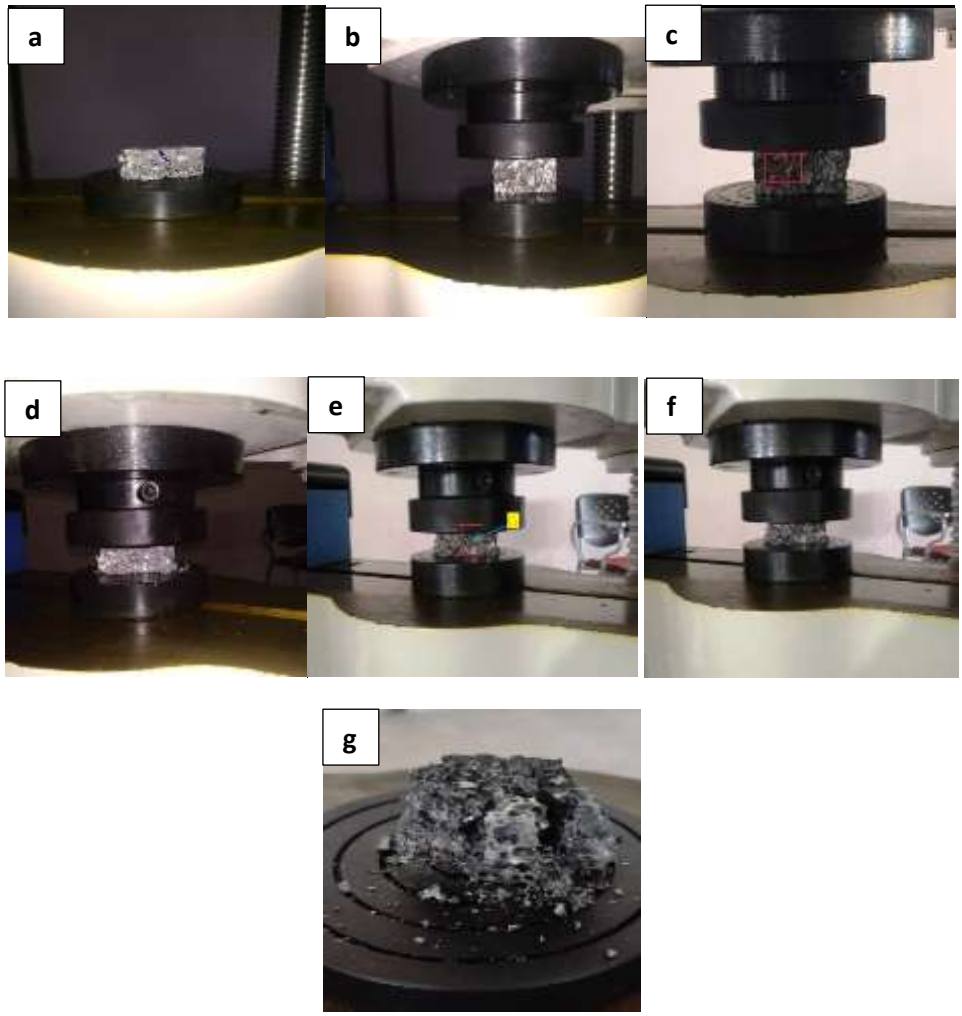

Figure 13 (B) Corresponding stages of deformation

In the compressive stress-strain curve, it is observed that the curve has three different deformation zones; Figure 13B (a) depicts the initial position (i.e., ε = 0 %) of the specimen mounted on the UTM and afterwards, the compressive loading started. As the compressive load increases gradually, the bending and stretching of specimen cell walls and cell faces occur, which is demonstrated by linear elastic region (i) in the stress-strain response and corresponding images of the specimen are represented in Figure 13B (b). This localized layer by layer deformation initiated inside the foam specimen from the upper surface (i.e. attached to the UTM anvil) to the lower surface after the homogeneous elastic deformation. Firstly, the bigger cells, close to the compressive loading face, start collapsing due to the large radius of the curvature cell wall; individual cell walls behave like plastic hinges and the bending of the cell wall initiated at the weaker section the cell wall. Figure 13B (c-e) shows the cracks (Represented in red box)) which are generated at some stage in the crushing and shearing of cell walls, and these crushed layer cells are close to the loading face are known as deformation bands (DB). This DB indicates that the deformation behavior of the specimen is layer by layer, and due to that, an almost constant plateau zone (ii) was observed in the stress-strain curve. At the higher strain values (≥40%) in the mid part of the specimen, foam cells initially get stretched and bent then, followed by shearing and crushing [Figure 13B (e)]. It is also found that the growth of present cracks leads to the cell walls of foam being fractured (marked by 'CF'). The AHCFs foam specimen gets starts to densify [Figure 13B (e)], and Lastly, AHCFs foam gets densified after it behaves like dense or solid material [Figure 13B (f)], which is indicated by the densification zone in the compressive stress-strain response (iii).

3.6.Cell wall hardness

A Rockwell hardness tester was employed to measure the hardness of each sample (indentation hardness) as shown in Table 4.

Table 4. Rockwell hardness of the samples

Sample	Average (HRB)
ACFs	23
AHCFS-1	49.34
AHCFs-2	54.23
AHCFS-3	58.5
AHCFS-4	73.4

The Rockwell hardness of samples without reinforcement (ACFs) and different percentages by weight of reinforcement of the hybrid composite were evaluated. It is seen that the hardness of unreinforced composite foam is much less than the hardness of reinforced hybrid composite foam. It can also observe that by increasing the weight percentage of reinforcement, the cell wall hardness of AHCFs increased.

4. CONCLUSION

Closed AHCF with different primary reinforcement SiC and 3 wt. % of secondary reinforcement (TiB_2) were fabricated by stir casting technique using oyster-shell powder as a foaming agent without a thickening agent. The effect of reinforcement content on the foam morphology, microstructure, physical properties, and compressive properties was studied.

1. AHCFs-1 (AA7075+3wt% SiC+3% TiB_2) has the lowest density and the highest foamability. The cell size was the largest in this foam, and the cell wall thickness was the thinnest. AHCFs-4 ((AA7075+12wt% SiC+3% TiB_2) has a higher density as compared to unreinforced (ACFs); this is due to the improper mixing of reinforcement which increases viscosity.
2. Reinforcement (SiC and TiB_2) content strongly influenced the physical and compressive responses of Aluminium Hybrid composite foams (AHCFs). The yield strength and σ_{pl} of AHCFs increase with the increases in SiC weight percentage. AHCFs-4 exhibited the highest elastic modulus yield strength and plateau strength and the highest density because of the lowest foamability.
3. Stirring temperature also strongly influenced the microstructural properties of AHCFs. It was observed that 750^0C of stirring temperature was sufficient for aluminium foaming. The change in physical properties of aluminium foam was trivial with an increase of stirring temperature beyond 750^0C.
4. The hardness of AHCFs on the cell wall increased with an increase in the weight percentage of reinforcement.
5. For AA7075 aluminium matrix composite foam, 3-9 wt. % of primary reinforcement (SiC) and 750^0C stirring temperature are suitable.
6. Deformation of AHCFs foams starts near the loading surface and proceeds to the bottom surface, and all types of AHCFs foams exhibit identical deformation behaviour.

Acknowledgment
The authors gratefully acknowledge the present work as part of research work funded by VIT Bhopal University under Support for Excellence in Academic Research (SPEAR) grant number SMG-01.

Conflict of Interest
The authors declare that they have no conflict of interest.

Data Availability
All data sources are described in this study are directed at the authors.

Code Availability
Not Applicable.s

Ethics Approval
No ethical issues arose during either the experimental process or the preparation of the manuscript.

Consent for Publication
All authors have given their consent to publish this manuscript.

Authors' Contribution

Nitish Kumar Singh: Fabrication, testing, Investigation, Resources, and Writing - original draft. Balaguru Sethuraman: Conceptualization, Supervision, Writing - review & editing.

REFERENCES

[1] T. K. Tatt, N. Muhamad, A. B. Sulong, S. Paramasivam, H. S. Huey, and S. A. Anuar, "Review on Manufacturing of Metal Foams," *ASM Sci. J.*, vol. 16, no. July, pp. 1–8, 2021, doi: 10.32802/asmscj.2021.794.

[2] B. Parveez, N. A. Jamal, A. Maleque, F. Yusof, N. H. Jamadon, and S. Adzila, "Review on advances in porous Al composites and the possible way forward," *Journal of Materials Research and Technology*, vol. 14. Elsevier Editora Ltda, pp. 2017–2038, Sep. 01, 2021, doi: 10.1016/j.jmrt.2021.07.055.

[3] R. K. Rathore, N. K. Singh, A. K. Sinha, K. Panthi, and A. K. Sharma, "Mechanical properties of lightweight aluminium hybrid composite foams (AHCFs) for structural applications," *Adv. Mater. Process. Technol.*, vol. 00, no. 00, pp. 1–15, 2022, doi: 10.1080/2374068X.2022.2048498.

[4] S. Sowmiya, P. Nallanukala, J. Anburaj, and B. Simhachalam, "Development of Metallic Aluminium Foam Casting Using Calcium Carbonate Precursors for Side Impact Beam Application," *Mater. Today Proc.*, vol. 5, no. 9, pp. 20362–20370, 2018, doi: 10.1016/j.matpr.2018.06.411.

[5] H. O. A. Osman, A. M. Omran, A. A. Atlam, and M. M. Kh, "Fabrication of aluminum foam from aluminum scrap Hamza," *Int. J. Eng. Res. Appl.*, vol. 5, no. 2, pp. 109–115, 2015.

[6] A. Uzun, "Production of aluminium foams reinforced with silicon carbide and carbon nanotubes prepared by powder metallurgy method," *Compos. Part B Eng.*, vol. 172, no. March, pp. 206–217, 2019, doi: 10.1016/j.compositesb.2019.05.045.

[7] Y. Hangai, T. Morita, and T. Utsunomiya, "Functionally graded aluminum foam consisting of dissimilar aluminum alloys fabricated by sintering and dissolution process," *Mater. Sci. Eng. A*, vol. 696, no. March, pp. 544–551, 2017, doi: 10.1016/j.msea.2017.04.070.

[8] R. Singh, R. Arora, and J. D. Sharma, "Effect of Solutionizing Time on Microstructure, Mechanical Properties and Energy Absorption Capacity of Al2024-B4CP Composite Foam," *Trans. Indian Inst. Met.*, 2022, doi: 10.1007/s12666-022-02563-z.

[9] E. Prados Martín, "Microstructural parameters affecting the compressive response of closed-cell aluminum foams," *Mech. Adv. Mater. Struct.*, vol. 0, no. 0, pp. 1–20, 2021, doi: 10.1080/15376494.2021.1872747.

[10] S. Báez–Pimiento, M. E. Hernández–Rojas, and M. E. Palomar–Pardavé, "Processing and Characterization of Open–Cell Aluminum Foams Obtained through Infiltration Processes," *Procedia Mater. Sci.*, vol. 9, pp. 54–61, 2015, doi: 10.1016/j.mspro.2015.04.007.

[11] J. Banhart, "Manufacture, characterisation and application of cellular metals and metal foams," *Prog. Mater. Sci.*, vol. 46, no. 6, pp. 559–632, 2001, doi: 10.1016/S0079-6425(00)00002-5.

[12] F. García-Moreno, "Commercial applications of metal foams: Their properties and production," *Materials (Basel).*, vol. 9, no. 2, pp. 20–24, 2016, doi: 10.3390/ma9020085.

[13] G. Srinath, A. Vadiraj, G. Balachandran, S. N. Sahu, and A. A. Gokhale, "Characteristics of aluminium metal foam for automotive applications," *Trans. Indian Inst. Met.*, vol. 63, no. 5, pp. 765–772, 2010, doi: 10.1007/s12666-010-0117-7.

[14] R. Karuppasamy and D. Barik, "Production methods of aluminium foam: A brief review," *Mater. Today Proc.*, no. xxxx, 2020, doi: 10.1016/j.matpr.2020.07.161.

[15] S. Sahu, M. Z. Ansari, and D. P. Mondai, "Microstructure and compressive deformation behavior of 2014 aluminium cenosphere syntactic foam made through stircasting technique," *Mater. Today Proc.*, vol. 25, no. xxxx, pp. 785–788, 2019, doi: 10.1016/j.matpr.2019.09.019.

[16] S. Birla, D. P. Mondal, S. Das, D. K. Kashyap, and V. A. N. Ch, "Effect of cenosphere content on the compressive deformation behaviour of aluminum-cenosphere hybrid foam," *Mater. Sci. Eng. A*, vol. 685, no. October 2016, pp. 213–226, 2017, doi: 10.1016/j.msea.2016.12.131.

[17] D. P. Mondal, M. D. Goel, V. Upadhyay, S. Das, M. Singh, and A. K. Barnwal, "Comparative Study on Microstructural Characteristics and Compression Deformation Behaviour of Alumina and Cenosphere Reinforced Aluminum Syntactic Foam Made Through Stir Casting Technique," *Trans. Indian Inst. Met.*, vol. 71, no. 3, pp. 567–577, 2018, doi: 10.1007/s12666-017-1211-x.

[18] M. R. Farahani, S. Hossein Elahi, and H. R. Rezaei Ashtiani, "Effect of Silicon Content on Mechanical Properties and Progressive Collapse Behavior of Closed-cell Aluminum Foams," *Trans. Indian Inst. Met.*, vol. 74, no. 12, pp. 3145–3154, 2021, doi: 10.1007/s12666-021-02390-8.

[19] B. N. Yadav, D. Muchhala, P. Singh, A. N. C. Venkat, and D. P. Mondal, "Synergic effect of MWCNTs and SiC addition on microstructure and mechanical properties of closed-cell Al–SiC-MWCNTs HCFs," *Compos. Part B Eng.*, vol. 172, pp. 458–471, 2019, doi: 10.1016/j.compositesb.2019.05.041.

[20] N. Singh, R. M. Belokar, and R. S. Walia, "Experimental Investigation on Microstructural and Mechanical Attributes of Al 7075-T6/SiC/CR/MoS2 Based Green Hybrid Composite Via Advanced Vacuum-Sealed Bottom Pouring Stir Casting," *Silicon*, 2021, doi: 10.1007/s12633-021-01473-x.

[21] R. K. Mandava, V. V. Reddy, V. R. K. Rao, and K. S. Reddy, "Wear and Frictional Behaviour of Al 7075/FA/SiC Hybrid MMC's Using Response Surface Methodology," *Silicon*, 2021, doi: 10.1007/s12633-021-01300-3.

[22] N. Sreedhar and S. Balaguru, "Mechanical and tribological behaviour of al 7075 hybrid mnc's using stir casting method," *Int. J. Mech. Prod. Eng. Res. Dev.*, vol. 10, no. 3, pp. 391–400, 2020, doi: 10.24247/ijmperdjun202036.

[23] M. K. Sahu and R. K. Sahu, "Experimental Investigation, Modeling, and Optimization of Wear Parameters of B4C and Fly-Ash Reinforced Aluminum Hybrid Composite," *Front. Phys.*, vol. 8, no. July, pp. 1–14, 2020, doi: 10.3389/fphy.2020.00219.

[24] R. K. Bhushan, S. Kumar, and S. Das, "Fabrication and characterization of 7075 Al alloy reinforced with SiC particulates," *Int. J. Adv. Manuf. Technol.*, vol. 65, no. 5–8, pp. 611–624, 2013, doi: 10.1007/s00170-012-4200-6.

[25] S. Ko *et al.*, "Fabrication of TiB2-Al1050 Composites with Improved Microstructural and Mechanical Properties by a Liquid Pressing Infiltration Process," *Materials (Basel).*, vol. 13, no. 7, 2020, doi: 10.3390/ma13071588.

[26] U. A. Atturan, S. H. Nandam, B. S. Murty, and S. Sankaran, “Processing and characterization of in-situ TiB2 stabilized closed cell aluminium alloy composite foams,” *Mater. Des.*, vol. 101, pp. 245–253, 2016, doi: 10.1016/j.matdes.2016.03.153.

[27] R. K. Rathore, N. K. Singh, and J. F. Xavier, “Characterization of AA7075 Alloy Foam Using Calcium and Magnesium Carbonate as Foaming Agent,” 2021, pp. 289–297.

[28] V. B.U, “Development of Aluminum Foams by Different Methods and Evaluation of its Density by Archimedes Principle,” *Bonfring Int. J. Ind. Eng. Manag. Sci.*, vol. 2, no. 4, pp. 148–152, 2012, doi: 10.9756/bijiems.1866.

[29] K. S. Verma, D. Muchhala, S. K. Panthi, and D. P. Mondal, “Influences of Cell Size, Cell Wall Thickness and Cell Circularity on the Compressive Responses of Closed-Cell Aluminum Foam and its FEA Analysis,” *Int. J. Met.*, 2021, doi: 10.1007/s40962-021-00627-2.

[30] D. P. Mondal, N. Jha, A. Badkul, B. Gul, S. Rathod, and S. Das, “Effect of age hardening on compressive deformation behavior of Al-alloy (LM13)-cenosphere hybrid foam prepared using CaCO3 as a foaming agent,” *J. Mater. Res.*, vol. 28, no. 17, pp. 2528–2538, 2013, doi: 10.1557/jmr.2013.197.